GSA DATA REPOSITORY 2013158

Supplementary Information for "Noble metals potential of sulfide-saturated melts from the subcontinental lithosphere"

V.S. Kamenetsky et al.

1. Liquidus assemblage of the melt S18-60/1

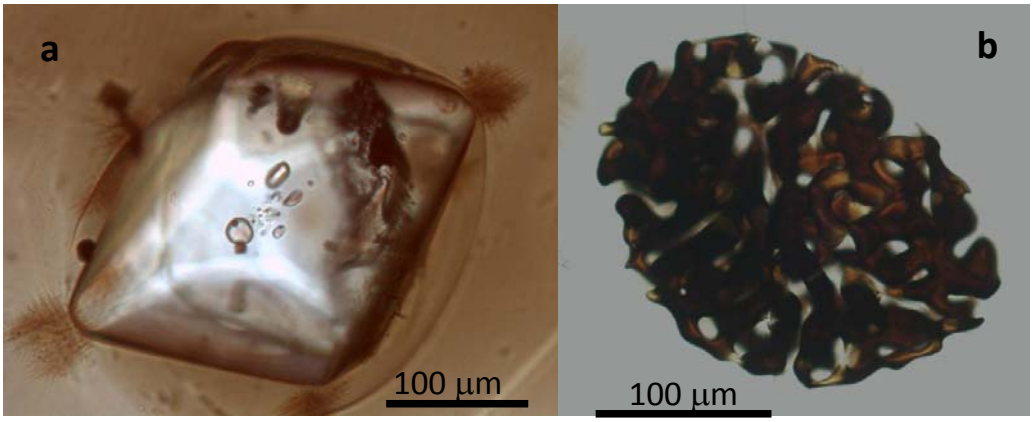

Figure DR1. Microphenocrysts of euhedral olivine containing primary glass inclusions (a) and skeletal Cr-spinel (b) in the BTJ glass

2. Methods and results

2.1. Re-Os and Hf isotope analyses for S18-60/1

Re–Os isotope data were obtained in 2001 at the University of Giessen, Germany, following established methods (Brauns, 2001; Brauns et al., 2000). After powdering in an agate mortar and pestle, ~119 mg of glass S18-60/1 was weighed into a pre-spiked ($^{185}Re/^{190}Os$ tracer ~ 300) Carius tube, followed by dissolution and equilibration with inverse aqua regia at 240°C. Osmium was extracted by distillation of the volatile tetra oxide, condensed on a very small volume (2 µl) of chilled H_2SO_4 and then collected in 0.5 ml of 6.8 N HBr. Final purification of Os was done by micro-distillation (Birck et al., 1997). Rhenium was separated from the matrix using Dowex 1X8 resin and a 'HNO_3 chemistry'. Os isotope ratios were measured by ion-counting on a modified Finnigan-MAT 261 operated in NTIMS mode; correction procedures for mass bias and oxides are based on ref. (Reisberg and Meisel, 2002). During the course of this work, DTM-Os yielded an average $^{187}Os/^{188}Os$ ratio of 0.17393 ± 38 (n = 5), consistent with published results from other laboratories (e.g. two sets of long term averages from DTM: 0.17429 ± 55, 0.17396 ± 38, (Shirey, 1997); two sets of averages from Monash University, Australia: 0.17367 ± 58, 0.17400 ± 21 (Lambert et al., 1998; McBride et al., 2001)). The Re isotope dilution analysis was performed using Faraday detectors on the same NTIMS instrument, with mass bias correction based on standard bracketing providing an internal (2se) precision of ±0.1%. Based on the isotope dilution results, the analysed aliquot of glass S18-60 (119 mg) contained ~50 pg Re and 1.6 pg Os. After correction for blank (Re 90% yield, 5 pg blank; Os 85% yield, 0.1±0.05 pg blank with $^{187}Os/^{188}Os$ ~0.108), overall uncertainties (including spike

calibration) are estimated to be ±1.3% (2 SD, $^{187}Re/^{188}Os$) and ±1% (2 SD, $^{187}Os/^{188}Os$). The blank-corrected Re-Os results are given in Table DR1.

The Hf isotope composition was measured at the University of Melbourne using established methods (Woodhead et al., 2001). Hf was extracted from ~40 mg of glass using a 2-column procedure modified from ref. (David et al., 1999) and measured on a NU Plasma MC-ICPMS. Mass bias was corrected by internal normalisation to $^{179}Hf/^{177}Hf$=0.7325 and the resulting $^{176}Hf/^{177}Hf$ is reported relative to JMC475=0.282160. External precision is ±0.000015 (2sd). Modern CHUR is assumed to have $^{176}Hf/^{177}Hf$ = 0.282772 (Blichert-Toft and Albarede, 1997). The Hf isotope results for S18-60/1 are given in Table DR2. Results for other isotopic systems (Sr, Nd, Pb, O) for glass S18-60/1 (Kamenetsky et al., 2001) are also listed in Table DR2.

Table DR1. Re-Os isotope data, S18-60/1

Re ppt	**±2s**	**Os ppt**	**±2s**	**$^{187}Re/^{188}Os$**	**±2s**	**$^{187}Os/^{188}Os$**	**±2s**
382	2	14	1	133	2	0.1655	0.0017

Table DR2. Hf and Sr-Nd-Pb-O isotope data, S18-60/1

Hf ppm	1.71
$^{176}Hf/^{177}Hf$	0.282045±8
ε_{Hf}	-25.7
Sr ppm	143
$^{87}Sr/^{86}Sr$	0.71209±3
Nd ppm	9.0
$^{143}Nd/^{144}Nd$	0.511663±20
ε_{Nd}	-19.0
Pb ppm	0.91
$^{206}Pb/^{204}Pb$	17.188±9
$^{207}Pb/^{204}Pb$	15.701±8
$^{208}Pb/^{204}Pb$	38.766±30
$\delta^{18}O$, ‰	6.8 ±0.2

Trace element concentrations and Sr-Nd-Pb-O are from (Kamenetsky et al., 2001). Errors given for Sr-Nd-Pb isotope results are external precision (2sd). $^{176}Hf/^{177}Hf$ reported relative to JMC475=0.282160. Sr-Nd-Pb isotope ratios measured by TIMS; $^{87}Sr/^{86}Sr$ is relative to SRM987=0.710230, $^{143}Nd/^{144}Nd$ is relative to LaJolla=0.511860, Pb isotope ratios corrected for mass bias using a ^{207}Pb-^{204}Pb double spike and reported relative to SRM981 16.935, 15.491, 36.701. $\delta^{18}O$ reported relative to V-SMOW and NBS28 = 9.58±0.12 permil.

2.2. Electron microprobe analysis of glass and minerals in S18-60/1

Major and trace elements were determined on a Jeol JXA 8200 SuperProbe Electron Probe Microanalyzer at the Max Planck Institute for Chemistry (Mainz, Germany).
Major-element abundances in glasses were measured at an accelerating voltage of 15 kV and a beam current of 12 nA with a reference sample of natural basaltic glass USNM111240/52 (VG2) (Jarosewich et al., 1980), with a relative error of 1–2%. The compositions of olivine and some elements in the glass were analysed at an accelerating voltage of 20 kV and a beam current of 300 nA for olivine and 200nA for the glass, following a special procedure which allows 20–30 ppm (two-

sigma error) precision and accuracy for Ni, Ca, Mn, Al, Ti, Cr, and 0.02 mole % for the forsterite component in olivine (Sobolev et al., 2007) and 20 ppm for Cl, Cr, K, S and 40 ppm for P in the glass. The data were corrected using routines ZAF procedure. A set of reference materials i.e., natural and synthetic oxides, mineral and glasses (P&H Developments Ltd., Calibration Standards for Electron Probe Microanalysis, Standard Block GEO, and the Smithsonian Institution standard set for electron microprobe analysis (Jarosewich et al., 1980) were used for routine calibration and instrument stability monitoring.

2.3. Raman analysis of sulfide globule in S18-60/1

The sample was analysed with a Renishaw inVia Raman Microscope using a Streamline map. The excitation wavelength was 532 nm using a 200 mW diode laser at 10% power and a 30 s exposure time was used for the line scan (note that the power is spread over >40 pixels). A grating of 600 l/mm was used covering a spectral range of 131 – 3698 cm^{-1}. An area of 127.2 x 117.6 µm, marked in Fig. S2, was collected using a 100x objective (Leica, N Plan Epi, NA 0.85) using a 0.6 µm step size yielding an image of 213x197 pixels.

Cosmic rays were removed using the Renishaw Wire software utilizing the nearest neighbour method. Every potential ray was visually inspected before removing it. In order to obtain good references for the component mapping the same software was used to reduce the noise by performing a PCA analysis. It was judged that 31 principal component were needed to fully describe the spectral data. Different regions of this map were then explored to obtain spectra that represent all the single mineral phases present in the sample. The spectra used are shown in Fig. DR3, individual spectra with peak picking are shown in Fig. DR4. A component (DCLS) analysis was then performed on the original map data (free of cosmic rays) using the Wire software and the above mentioned reference spectra which were mean centred and scaled to unit variance. A lack-of-fit map was also created showing that no other significant areas have been left out that are not covered the chosen six components. The resulting component map is shown in Fig. DR5. For this image the boundaries of the components have been chosen in the look up table so that little overlap exists between the phases. In reality most Raman pixels are a complex mixture of several of the six components and an estimate of the component fractions was calculated which is a true reflection of the contribution of each these components. The calculations gave 14.33% for blue, 28.83% for cyan, 18.74 for red, 4.69% for green, 17.99% for grey and 15.43% for yellow.

A typical spectrum of the yellow/grey phase is shown in Fig. DR6 which is mostly a mixture of disordered goethite or feroxyhyte (de Faria et al., 1997; Smith et al., 1999) and magnetite (de Faria et al., 1997). The spectrum also shows a broad peak between 3000 and 3700 cm^{-1}, indicating the presence of OH. A curve fit was performed for this broad peak and saved as a separate reference spectrum. A component (DCLS) analysis was performed on the original map data (free of cosmic rays) using only this reference spectrum. The resulting map is shown in Fig. DR6 showing distribution of OH. This OH could either be from the disordered goethite or free water. There is a lack of information in the literature about the spectral Raman region above 2000 cm^{-1} of goethite and an in-house Goethite reference was measured using the same conditions as stated above. The spectrum is shown in Fig. DR6 and shows an absence of a broad peak between 3000 and 3700 cm^{-1} indicating that the OH peak in Fig. DR6 is the result of water. This could also explain the formation of cracks in this phase after the Raman mapping. The local heat of the Raman laser must have dehydrated this phase which led to the formation of visible cracks. Possible sample decomposition of the disordered goethite/feroxyhyte that is due to intense laser excitation can be ruled out as the Raman bands of

hematite, the product of goethite dehydration (de Faria et al., 1997), are not present in the map data. However, in a separate experiment a local spot of the FeO(OH) phase in the sulfide was exposed to 10% laser power (point analysis) for 120 s and the resulting spot clearly showed the presence of hematite afterwards, Fig. DR9.

A 64-bit version of Cytospec was also used to perform a Hierarchical Clustering analysis. The noise reduced map data was imported into Cytospec. The Hierarchical Cluster analysis used D-values for the distance calculations and the Ward's algorithm for the clustering. Seven clusters were chosen and the map is shown in Fig. DR10. The average spectrum of the pink cluster is very similar to the green cluster but does contain a series of artefacts which stem from artefacts of the cosmic ray removal. In essence this cluster should be ignored. The remaining six clusters resemble the component map.

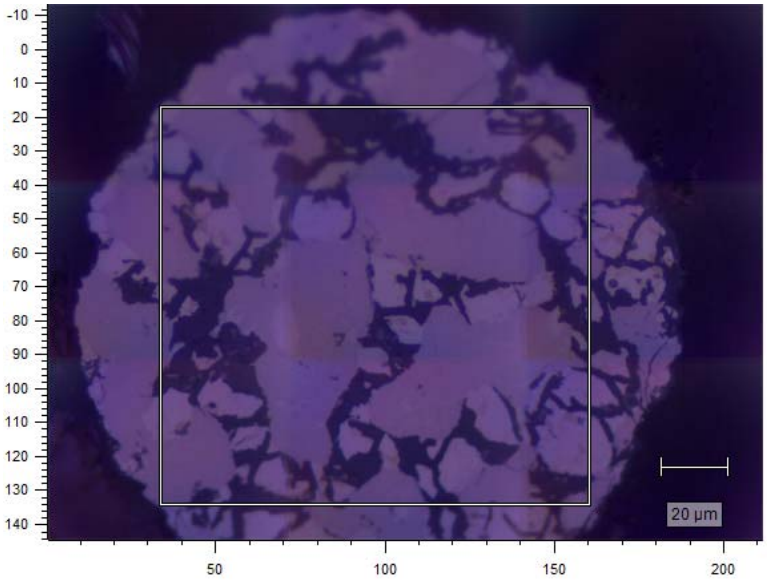

Figure DR2. White border outline of Raman map over visual image of the sulfide globule.

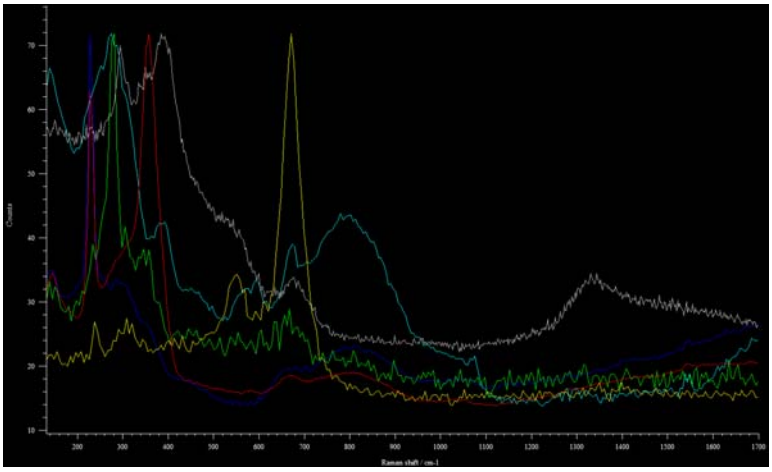

Figure DR3. Overlap of reference spectra used for component map, using same colours as component map: grey – (disordered goethite or feroxyhyte) (de Faria et al., 1997; Smith et al., 1999) yellow – (magnetite) (de Faria et al., 1997), other colours – unclassified

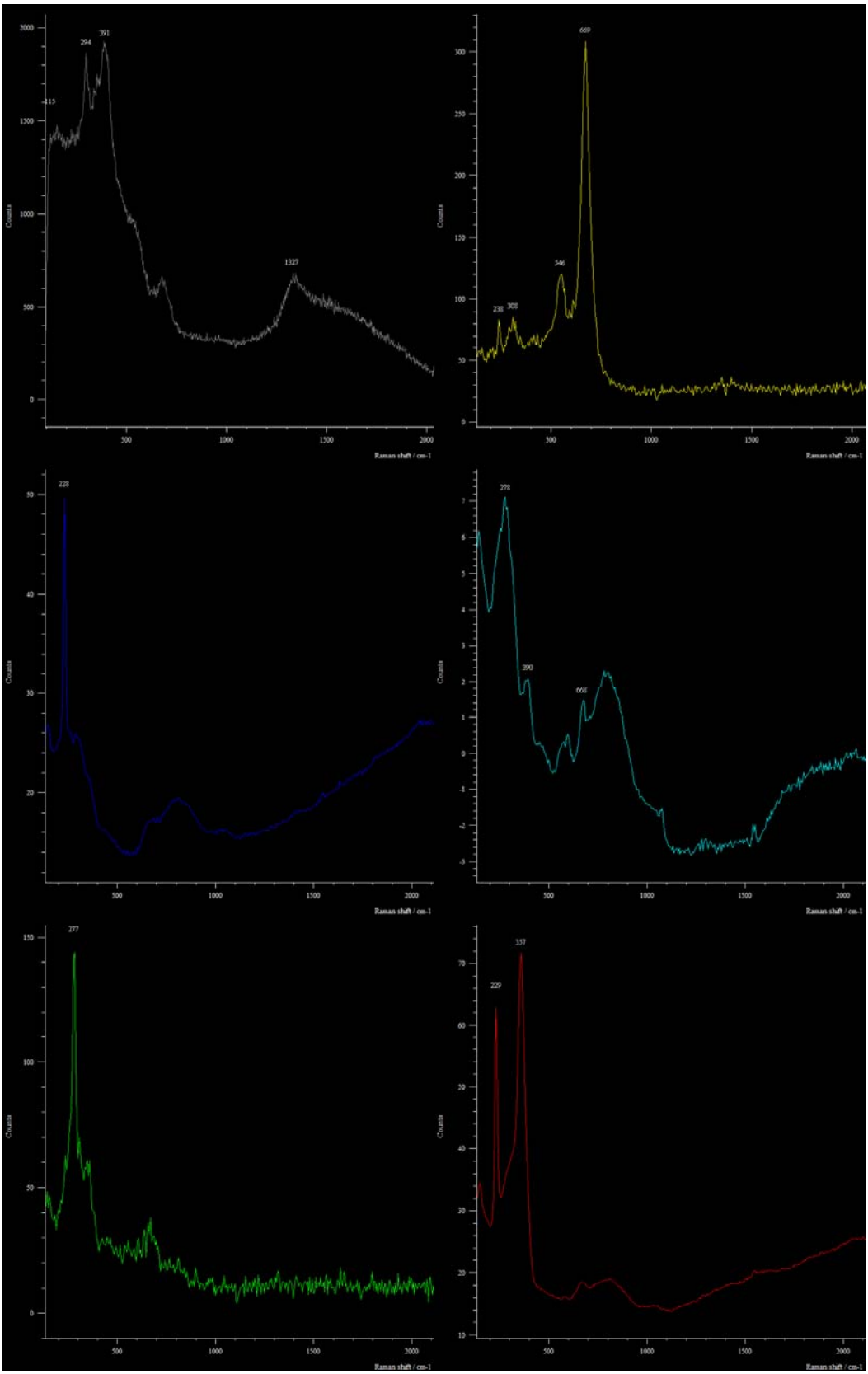

Figure DR4. Reference spectra of component map with peak picking

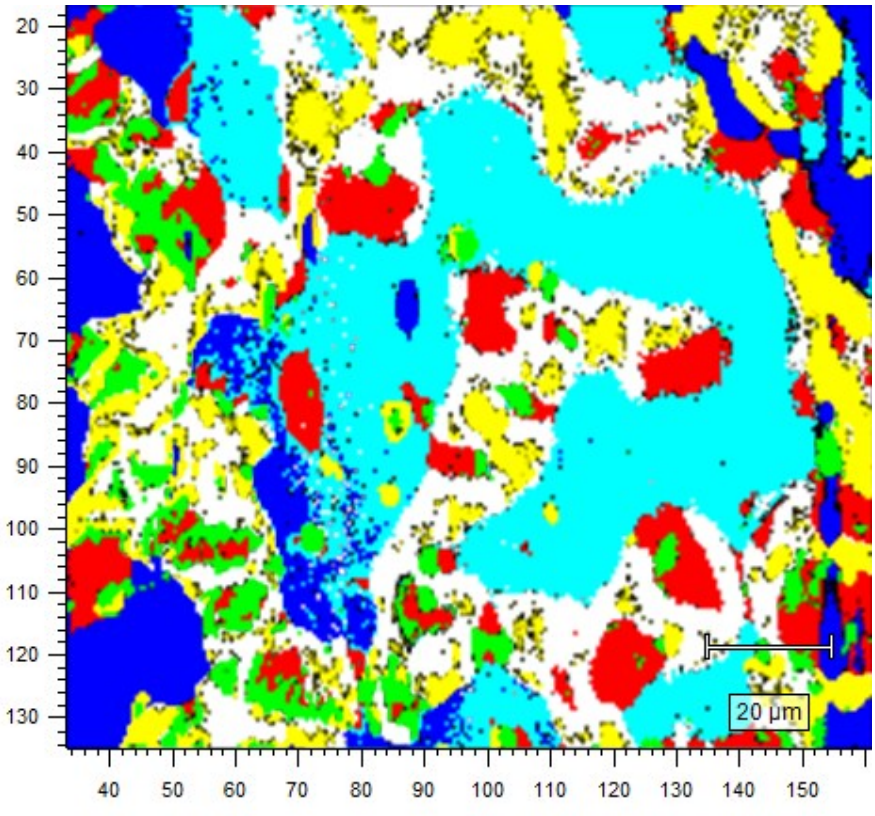

Figure DR5. Component map of the sulfide globule

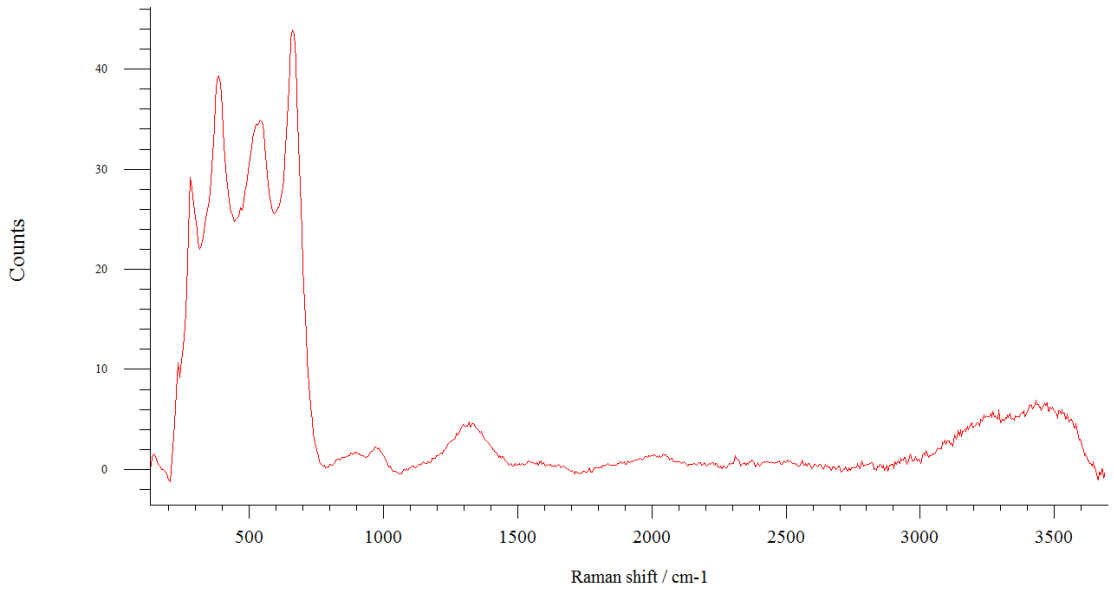

Figure DR6. Typical spectrum of the grey/yellow phase consisting mostly of goethite/ feroxyhyte and magnetite with a broad OH peak between 3000 and 3700 cm^{-1}

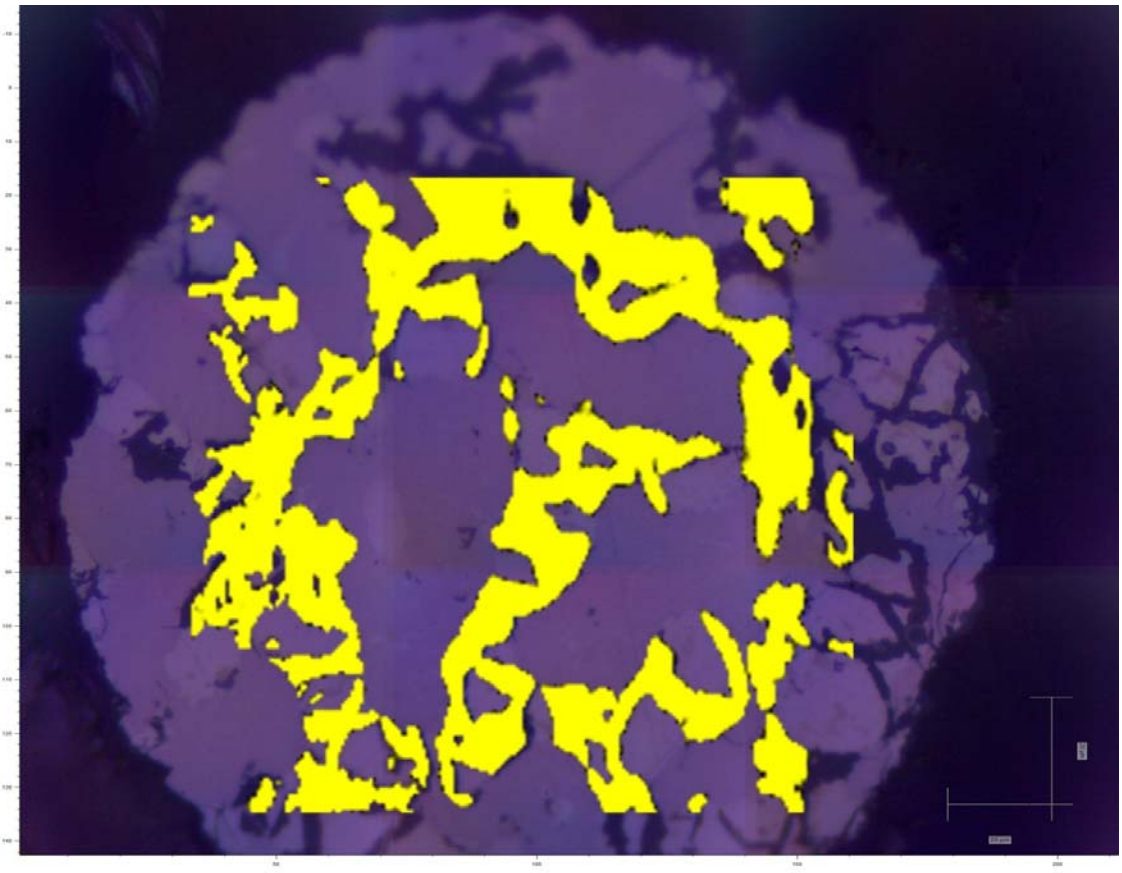

Figure DR7. Component map showing OH distribution in the sulfide globule

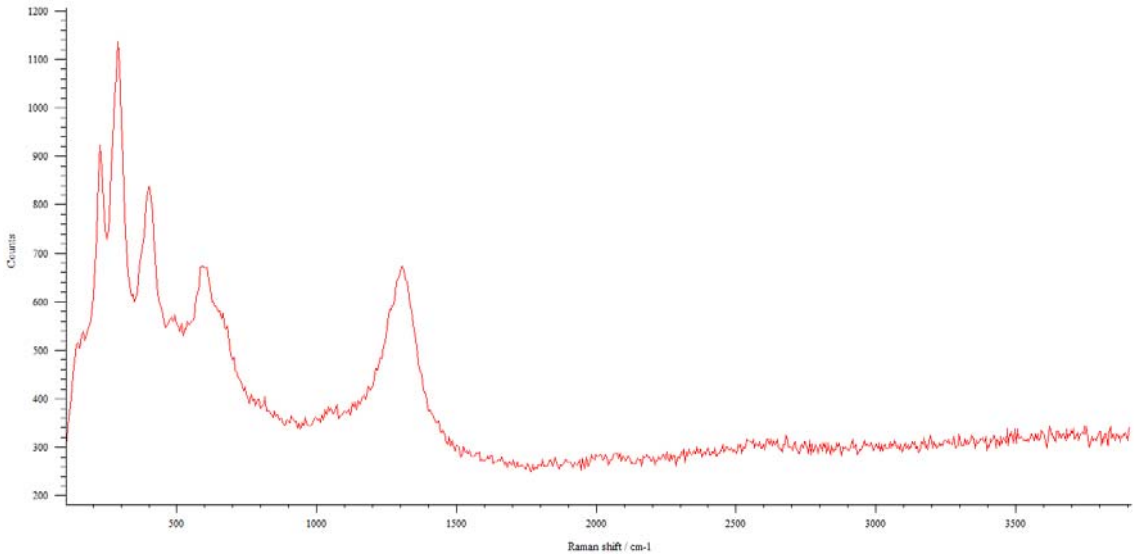

Figure DR8. Goethite reference supplied by School of Earth Sciences, University of Tasmania

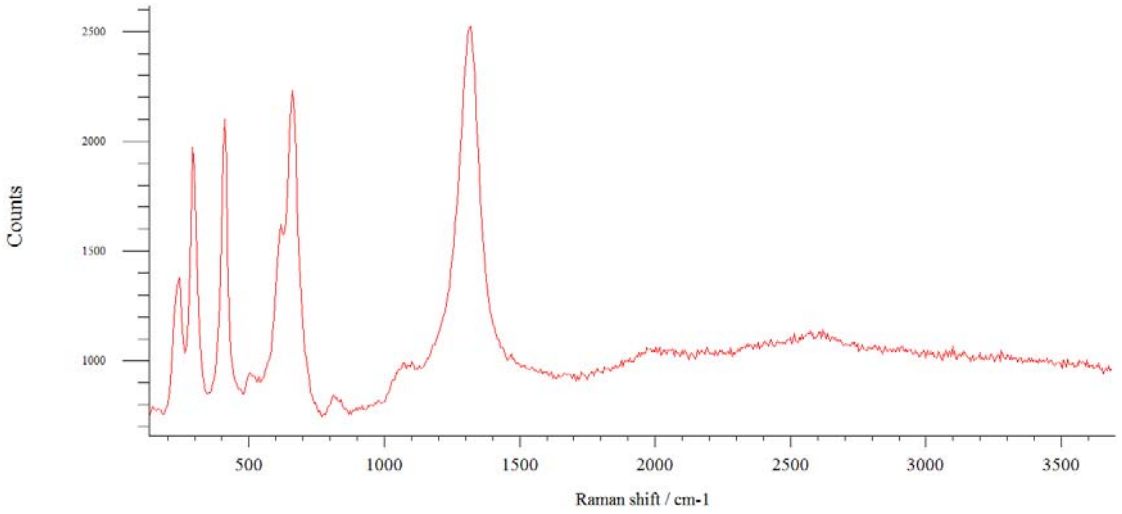

Figure DR9. Formation of hematite as a result of intense laser excitation of the FeO(OH) phase

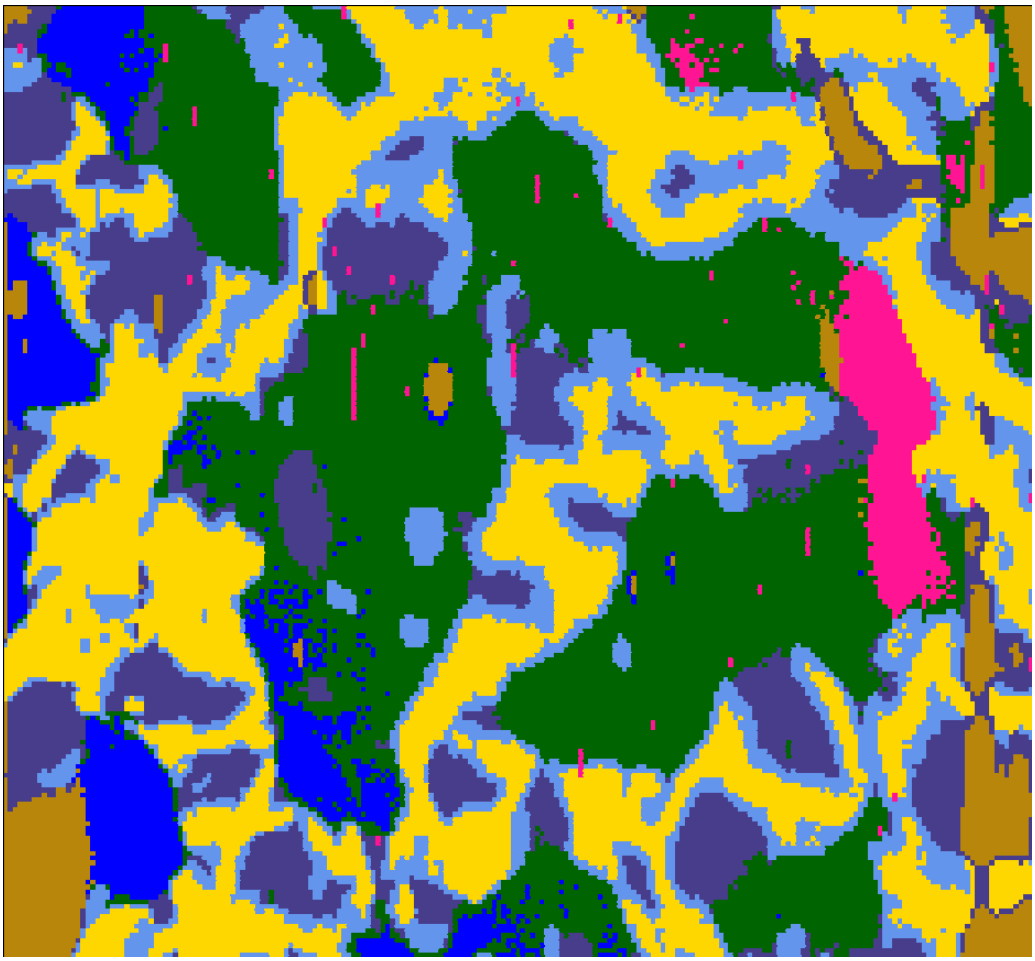

Figure DR10. Hierarchical cluster map showing seven clusters

2.4. Laser ablation ICPMS analysis of sulfide globule in S18-60/1

LA-ICPMS analysis of the glass was done using a Resonetics M50-E ArF excimer laser operated at a wavelength of 193nm, a repetition rate of 10Hz a spot size of 75µm and fluence of 5.5–6 J/cm^2 for glasses. The sulfide droplet was analysed by carrying out traverses (Fig. DR11) that started from glass at a rate of 5 µm /s, 7Hz repetition rate and a spot size of 55 µm and a fluence of 4 J/cm^2. Data were collected using a Thermo Fisher ELEMENT XR SC-ICPMS in time-resolved mode with 20 s measurement of the pure gas background, followed by 40 s of measurement during laser ablation and followed by 20 s measurement of pure gas background after laser ablation stopped. Count rates were measured using the following isotopes: ^{33}S, ^{43}Ca, ^{52}Cr, ^{53}Cr, ^{57}Fe, ^{59}Co, ^{60}Ni, ^{63}Cu, ^{65}Cu, ^{68}Zn, ^{75}As, ^{77}Se, ^{95}Mo ^{101}Ru, ^{102}Ru, ^{103}Rh, ^{105}Pd,^{106}Pd, ^{107}Ag,^{111}Cd, ^{115}In, ^{117}Sn, ^{119}Sn, ^{120}Sn, ^{121}Sn, ^{123}Sn, ^{185}Re, ^{184}W, ^{185}Re, ^{189}Os, ^{193}Ir, ^{194}Pt, ^{195}Pt, ^{197}Pt, ^{206}Pb, ^{207}Pb, ^{208}Pb, and ^{209}Bi. Count rates were then normalised to an internal standard (^{43}Ca for glass, ^{57}Fe for sulfide) and quantified using NIST-SRM 612 and a PGE Ni-rich sulfide standard (Wohlgemuth-Ueberwasser et al., 2007) for the glass and sulfide droplet respectively. The trace element composition (in ppm) of the sulfide is present in Table DR3.

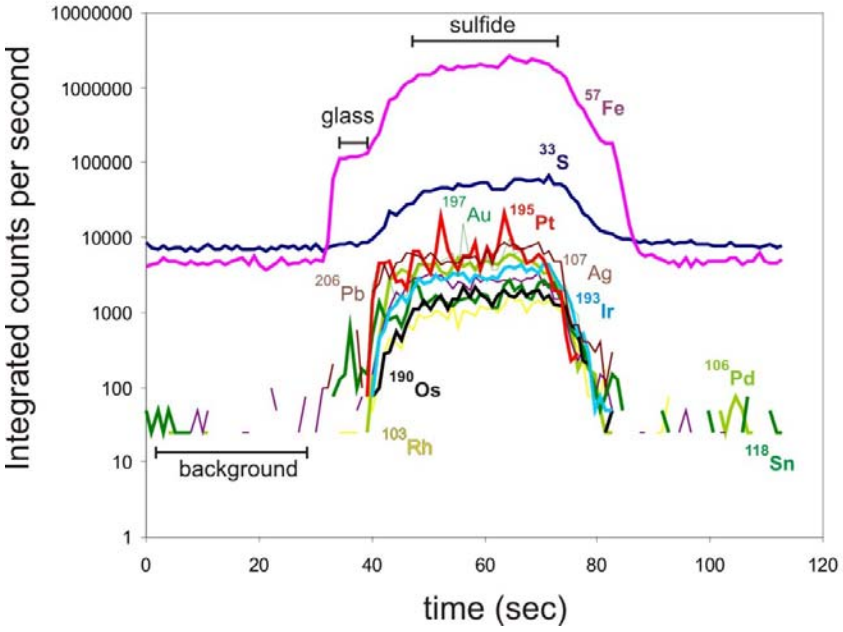

Figure DR11. Time-resolved signal (y axis, counts per second) recorded for selected elements (masses) across the host glass – sulfide globule interfaces, analysed by laser ablation inductively coupled plasma-mass spectrometry.

Table DR3. Trace element composition of the BTJ sulfide globule

	Co	Cu	Zn	As	Se	Mo	Ru	Rh	Pd	Ag
ppm	1250	16480	262	37	116	31	14.8	2.98	41.3	15.2
1σ	230	3585	48	8	25	4	0.6	0.02	3.5	2.5

	Cd	In	Sn	W	Re	Os	Ir	Pt	Au	Pb	Bi
ppm	7.5	1.4	11.2	0.17	0.1	7.5	7.0	45.5	14.3	39.0	3.1
1σ	1.1	0.2	2.3	0.02	0.1	1.5	0.7	7.7	0.4	10.4	0.6

References

Birck, J.-L., Roy-Barman, M., and Capmas, F., 1997, Re–Os isotopic measurements at the femtomole level in natural samples: Geostandards Newsletter, v. 20, p. 19-27.

Blichert-Toft, J., and Albarede, F., 1997, The Lu-Hf isotope geochemistry of chondrites and the evolution of the mantle-crust system: Earth and Planetary Science Letters, v. 148, p. 243-258.

Brauns, C.M., 2001, A rapid, low blank technique for the extraction of osmium from geological samples: Chemical Geology, v. 176, p. 379–384.

Brauns, C.M., Hergt, J.M., Woodhead, J.D., and Maas, R., 2000, Os isotopes and the origin of the Tasmanian Dolerites: Journal of Petrology, v. 41, p. 905–918.

David, K., Birck, J.-L., Telouk, P., and Allègre, C.J., 1999, Application of isotope dilution for precise measurement of Zr/Hf and $^{176}Hf/^{177}Hf$ ratios by mass spectrometry (ID-TIMS/ID-MC-ICP-MS): Chemical Geology, v. 157, p. 1-12.

de Faria, D.L.A., Silva, S.V., and de Oliveira, M.T., 1997, Raman microspectroscopy of some iron oxides and oxyhydroxides: Journal of Raman Spectroscopy, v. 28, p. 873-878.

Jarosewich, E.J., Nelen, J.A., and Norberg, J.A., 1980, Reference samples for electron microprobe analysis: Geostandards Newsletter, v. 4, p. 43-47.

Kamenetsky, V.S., Maas, R., Sushchevskaya, N.M., Norman, M., Cartwright, I., and Peyve, A.A., 2001, Remnants of Gondwanan continental lithosphere in oceanic upper mantle: Evidence from the South Atlantic Ridge: Geology, v. 29, p. 243-246.

Lambert, D.D., Foster, J.G., Frick, L.R., Hoatson, D.M., and Purvis, A.C., 1998, Application of the Re–Os isotopic system to the study of Precambrian magmatic sulphide deposits of Western Australia: Australian Journal of Earth Sciences, v. 45, p. 265–284.

McBride, J.S., Lambert, D.D., Nicholls, I.A., and Price, R.C., 2001, Osmium isotopic evidence for crust-mantle interaction in the genesis of continental intraplate basalts from the Newer Volcanics Province, Southeastern Australia: Journal of Petrology, v. 42, p. 1197-1218.

Reisberg, L., and Meisel, T., 2002, The Re-Os isotopic system: a review of analytical techniques: Geostandards Newsletter, v. 26, p. 249– 267.

Shirey, S.B., 1997, Re-Os isotopic composition of mid-continent rift system picrites: implications for plume-lithosphere interaction and enriched mantle sources: Canadian Journal of Earth Sciences, v. 34, p. 489-503.

Smith, D.C., Bouchard, M., and Lorblanchet, M., 1999, An initial Raman microscopic investigation of prehistoric rock art in caves of the Quercy District, S. W. France: Journal of Raman Spectroscopy, v. 30, p. 347-354.

Sobolev, A.V., Hofmann, A.W., Kuzmin, D.V., Yaxley, G.M., Arndt, N.T., Chung, S.-L., Danyushevsky, L.V., Elliott, T., Frey, F.A., Garcia, M.O., Gurenko, A.A., Kamenetsky, V.S., Kerr, A.C., Krivolutskaya, N.A., Matvienkov, V.V., Nikogosian, I.K., Rocholl, A., Sigurdsson, I.A., Sushchevskaya, N.M., and Teklay, M., 2007, The amount of recycled crust in sources of mantle-derived melts: Science, v. 316, p. 412-417.

Wohlgemuth-Ueberwasser, C.C., Ballhaus, C., Berndt, J., Stotter née Paliulionyte, V., and Meisel, T., 2007, Synthesis of PGE sulfide standards for laser ablation inductively coupled plasma mass spectrometry (LA-ICP-MS): Contributions to Mineralogy and Petrology, v. 154, p. 607–617.

Woodhead, J.D., Hergt, J.M., Davidson, J.P., and Eggins, S.M., 2001, Hafnium isotope evidence for 'conservative' element mobility during subduction zone processes: Earth and Planetary Science Letters, v. 192, p. 331-346.